Additional information on the experimental methods

MCASSIGN Calculations and Resonance Assignments

Resonance peaks were picked manually from the 3D NCACX, NCOCX, and CONCA spectra in Sparky (1). 37, 38, and 42 sets of signals were identified for the NCACX, NCOCX, and CONCA spectra, respectively. The data were used to create signal tables for use with the MCASSIGN (2) program for computationally aided resonance assignment. Residue type assignments for the signals were chosen based on the carbon chemical shift frequencies. The D290 signals in the NCACX, NCOCX, and CONCA spectra were used to initiate assignments. The calculations were performed in three stages. First uncertainties of 0.4 ppm for ^{13}C and 0.5 ppm for ^{15}N were assigned to most signals. Larger uncertainties for several signals (0.6-1.0 ppm) were used based on linewidth and signal to noise in the 3D NMR experiments. MCASSIGN was run with weights for the 'Good', 'Bad', 'Edge', and 'Used' set at 0-10, 10-60, 0-5, and 0-2, respectively. 50-500 steps were calculated with 10^8 iterations per step for 50 independent runs of the MCASSIGN algorithm. Unique and definite signal assignments (i.e. the same signal assignment was obtained in > 90% of the runs and the residue was never assigned to two different signals) were obtained for residues Y288-F291, P298-N300, 303-308, and N314-Y319. In the next round of MCASSIGN calculations, the ^{13}C and ^{15}N uncertainties for the unassigned residues were reduced by 0.1 ppm and the calculations performed again. Definite assignments were obtained for residues G286-N287 and F309. In the third and final round of calculations, the uncertainties were increased by 0.1 ppm and definite assignments were obtained for residues S285 and G292-Y294.

Mass-Per-Length Measurement

6 nm carbon films were prepared on 300 mesh lacey copper grids (Electron Microscopy Sciences) and glow discharged immediately prior to use. 10 µl of the polymer solution was added to 90 µl of dialysis buffer and vortexed briefly. 5 µl of the diluted mCherry-hnRNPA2-LC wild-type polymers was incubated on the TEM grid along with 5 µl of dilute TMV solution (kindly provided by Dr. Gerald Stubbs, Vanderbilt University) for 3 min. The grid was blotted with a laboratory tissue and washed twice with 5 µl of deionized water before allowing to dry. Dark-field TEM images were recorded using the bottom mount camera of a Morgagni FEI microscope operating at 80 kV with a 1.2° tilted beam and following the procedure previously described (3). Images were analyzed in ImageJ (https://imagej.nih.gov/ij). MPL counts were determined according to the equation:

$$MPL = \frac{131}{I_{TMV}} \cdot \left(I_F - \frac{I_{B1} + I_{B2}}{2} \right)$$

Where I_{TMV} is the average integrated intensity of the TMV particles after background subtraction, I_F is the integrated intensity of a 60 nm X 80 nm rectangle centered on a mCherry-hnRNPA2-LC polymer, and I_{B1} and I_{B2} are the integrated intensities of the background on either side of the polymer. 131 kDa/nm is the known MPL value for TMV particles. A total of 655 polymer and 119 TMV MPL counts were obtained from 37 dark-field images. MPL error counts were determined using the equation:

$$Error = \frac{131}{I_{TMV}} \cdot \sqrt{\frac{3}{2}} \cdot (I_{B1} - I_{B2})$$

Where I_{B1} and I_{B2} are the integrated background intensities in a 60 nm X 80 nm rectangle that correspond to the same I_F integration discussed above, and I_{TMV} is the same as defined above. Data analysis and plotting was performed in Igor Pro 6.3.7.2 (WaveMetrics).

To quantify the relative amounts of truncated and full length mCherry-hnRNPA2-LC that contribute to the MPL measurement shown in Fig. 4E, a 200 µl aliquot of the polymer solution was centrifuged at 16,000 g for ~3 hr. The supernatant was removed and the pellet was dissolved in 200 µl of 6M guanidinium-HCl, 20 mM sodium phosphate pH 7.4. The solution was diluted by another factor of 2 before LC-MS analysis. 10 µl of the diluted solution was loaded onto a LC-MSQ+ system (ThermoScientific) and run at a flow rate of 0.2 ml/min over a C4 column (ThermoScientific) using water/acetonitrile solvents with 0.01% trifluoroacetic acid. The gradient was 5-60% acetonitrile over 30 min. The MSQ+ was operated in positive ion mode. The m/z data were analyzed in XCalibur (ThermoScientific) and MagTranZ (4). The mixture was determined to be 55% full length mCherry-hnRNPA2-LC (MW 45.8 kDa) and 45% truncated mCherry-hnRNPA2-LC (MW 34.7 kDa) giving an apparent MW of 40.8 kDa. The LC elution profile and MS deconvolution spectra are shown in SI Appendix, Fig. S10.

For the mCherry-hnRNPA2-LC D290V mutant MPL measurement shown in Fig. 4F, 3 µl of the polymer suspension was then applied to a 3 nm carbon film on a 300 mesh lacey carbon grid (Electron Microscopy Sciences) along with a 7 µl aliquot of dilute TMV solution and allowed to incubate for 3 min before blotting with a laboratory tissue and washing twice with 5 µl of deionized water and allowed to dry. The dark-field TEM images and image analysis were performed in the same manner as the mCherry-hnRNPA2-LC wild-type polymers. A total of 937 mCherry-hnRNPA2-LC D290V polymer and 83 TMV integrations from 82 images were performed to produce the histograms in Figs. 4F and S9E.

Solubility assay

500 µl of GFP-hnRNPA2-LC wild-type and D290V mutant protein in buffer containing 3 M urea, 20 mM Tris-HCl (pH 7.5), 200 mM NaCl, 20 mM BME, 0.5 mM EDTA, and 0.1 mM PMSF at 134 and 127 µM, respectively, was loaded onto 3 kDa MWCO, 500 µl, Amicon Ultra spin filters and concentrated to ~50 µl. The protein was harvested using a pipette and the filters were washed with 450 µl of 50 mM Tris-HCl, 200 mM sodium chloride, and 10 mM dithiothreitol and added to the concentrated protein. The mixture was vortexed extensively for 30 s and then rotated at room temperature for 7-9 days. Polymers were observed in each sample by negative stain TEM. 7 x 70 µl aliquots of each sample were harvested by centrifugation at 386,000 g for 2 hours at 22 °C. The supernatants were removed and the pellets were resuspended in the same buffer with urea concentrations of: 2.0, 2.5, 3.0, 3.5, 4.0, 4.5, and 5.0. The samples were rotated at room temperature for 21-22 h and then centrifuged at 386,000 g for 1 h at 22 °C. The supernatants were loaded into LC/MS vials and 100 µl of each sample was run on a C4 column (ThermoScientific) with a water/acetonitrile gradient (with 0.01% trifluoroacetic acid) of 5-60% over 30 min with a flow rate of 0.2 ml/min. The peak at 280 nm was integrated for each sample and converted to concentration using a calculated ε_{280} of 53,305 $M^{-1}cm^{-1}$ for both the

wild-type and D290V mutant proteins (SI Appendix, Fig. S12). The data in Fig. 5B are the average of two independent experiments. Errors bars are relative errors calculated using the average values of the seven data points at each urea concentration in the two experiments.

We assume that the polymers have reached steady-state equilibrium with protein monomers exchanging with the polymer ends (5):

$$[F] \underset{k_{on}}{\overset{k_{off}}{\rightleftarrows}} = [F] + [M]$$

Where $[F]$ is the concentration of polymer ends, $[M]$ is the protein monomer concentration, k_{off} is the monomer dissociation rate, and k_{on} is the monomer association rate. The above model indicates that at equilibrium the free monomer concentration, $[M]_e$, is simply the dissociation constant, K_D, and related to the free energy of monomer dissociation, ΔG, by:

$$[M]_e = e^{-\frac{\Delta G}{RT}}$$

Where R is the ideal gas constant and T is the temperature. We use the linear model for protein stability in the presence of denaturant (6):

$$\Delta G = \Delta G_0 - m[U]$$

Where m an interaction parameter of denaturant with protein and $[U]$ is the denaturant concentration. The data were plotted in Igor Pro 6.3.7.2 (WaveMetrics) and simultaneously fit to the function below with independent ΔG_0 values and a shared m parameter:

$$[M]_e = e^{-\frac{\Delta G_0}{RT}} e^{-\frac{m[U]}{RT}}$$

References

1. Goddard T & Kneller D (2008) SPARKY 3. *University of California, San Francisco*.
2. Hu K-N, Qiang W, & Tycko R (2011) A general Monte Carlo/simulated annealing algorithm for resonance assignment in NMR of uniformly labeled biopolymers. *Journal of Biomolecular NMR* 50(3):267-276.
3. Chen B, Thurber KR, Shewmaker F, Wickner RB, & Tycko R (2009) Measurement of amyloid fibril mass-per-length by tilted-beam transmission electron microscopy. *Proc Natl Acad Sci U S A* 106(34):14339-14344.
4. Zhang Z & Marshall AG (1998) A universal algorithm for fast and automated charge state deconvolution of electrospray mass-to-charge ratio spectra. *Journal of the American Society for Mass Spectrometry* 9(3):225-233.
5. O'Nuallain B, Shivaprasad S, Kheterpal I, & Wetzel R (2005) Thermodynamics of Aβ(1−40) Amyloid Fibril Elongation. *Biochemistry* 44(38):12709-12718.
6. Greene RF & Pace CN (1974) Urea and Guanidine Hydrochloride Denaturation of Ribonuclease, Lysozyme, α-Chymotrypsin, and β-Lactoglobulin. *Journal of Biological Chemistry* 249(17):5388-5393.


hnRNPA1 243-GY-NGFGND--GS--NFGGGGSYNDFGNYNN-QSSNFGPMKGGNFGG-283
hnRNPA2 270-GYGGGYDNYG-GG--NYGSGN-YNDFGNYNQ-QPSNYGPMKSGNFGG-311
hnRNPDL 357-GYGN-Y-NSAYGGDQNYSGYGGY-DYTGYNYGNYG-YGQGYA-DYSG-398

Figure S1

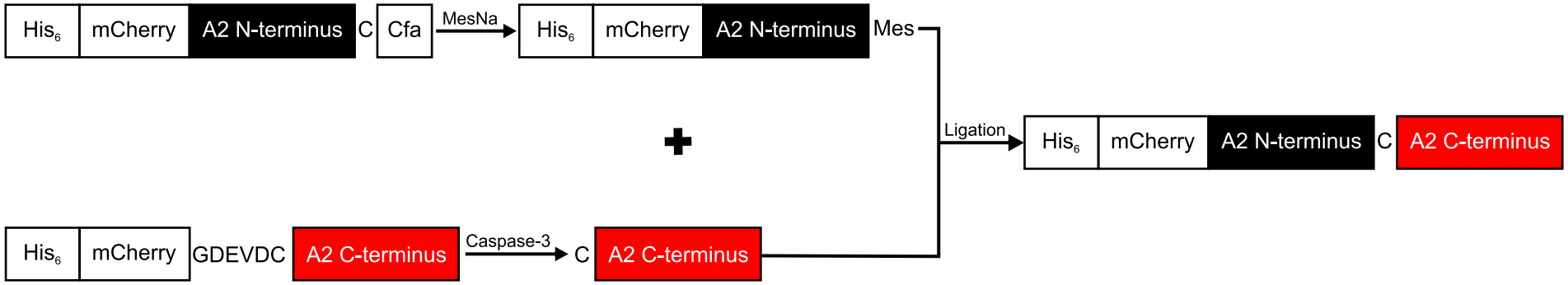
His6
mCherry
A2 N-terminus
C
Cfa
MesNa
His6
mCherry
A2 N-terminus
Mes
Ligation
His6
mCherry
A2 N-terminus
C
A2 C-terminus
His6
mCherry
GDEVDC
A2 C-terminus
Caspase-3
C
A2 C-terminus

Figure S2

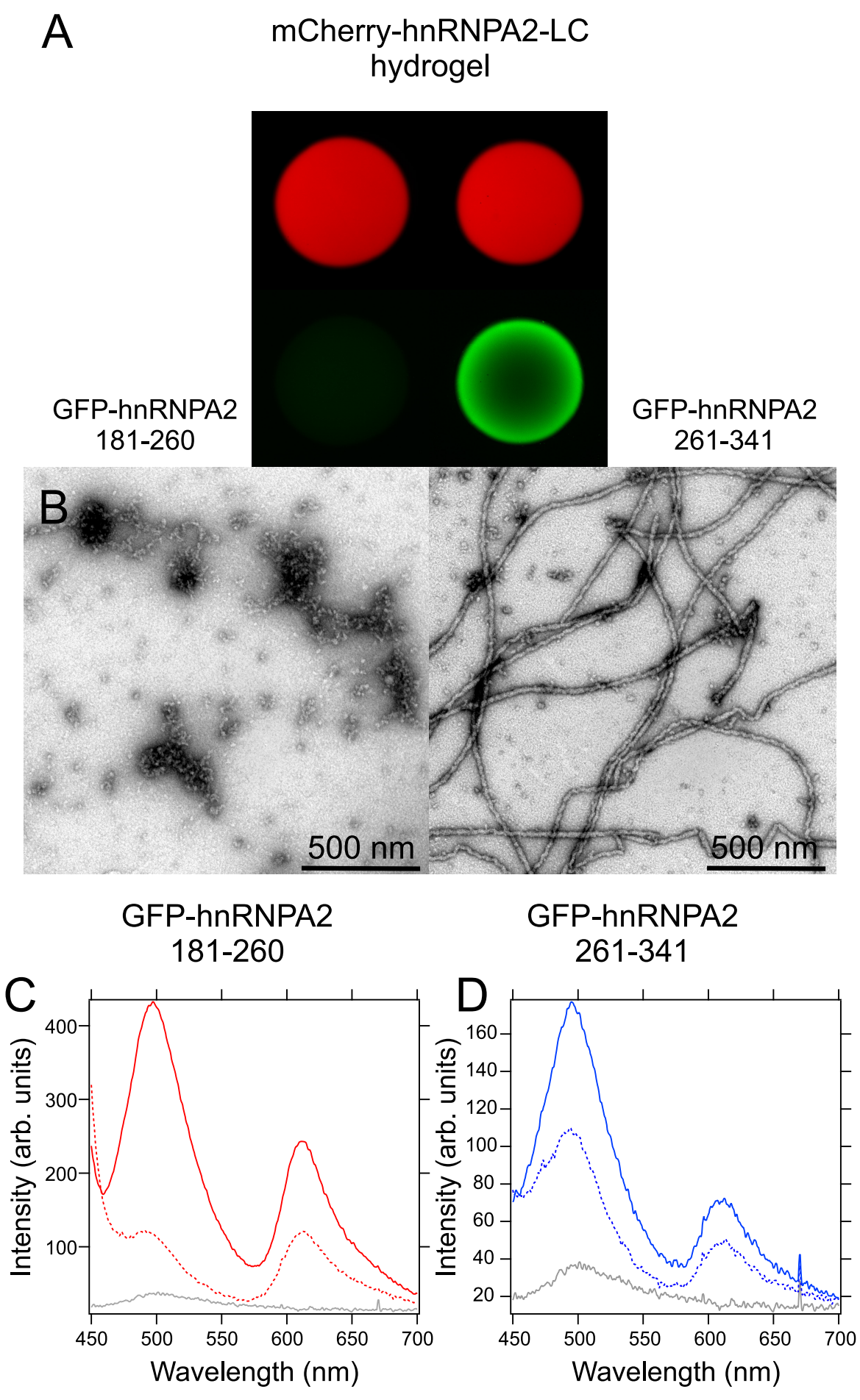
A
mCherry-hnRNPA2-LC
hydrogel
GFP-hnRNPA2
181-260
GFP-hnRNPA2
261-341
B
500 nm
500 nm
GFP-hnRNPA2
181-260
GFP-hnRNPA2
261-341
C
D
Intensity (arb. units)
Wavelength (nm)
Intensity (arb. units)
Wavelength (nm)

Figure S3

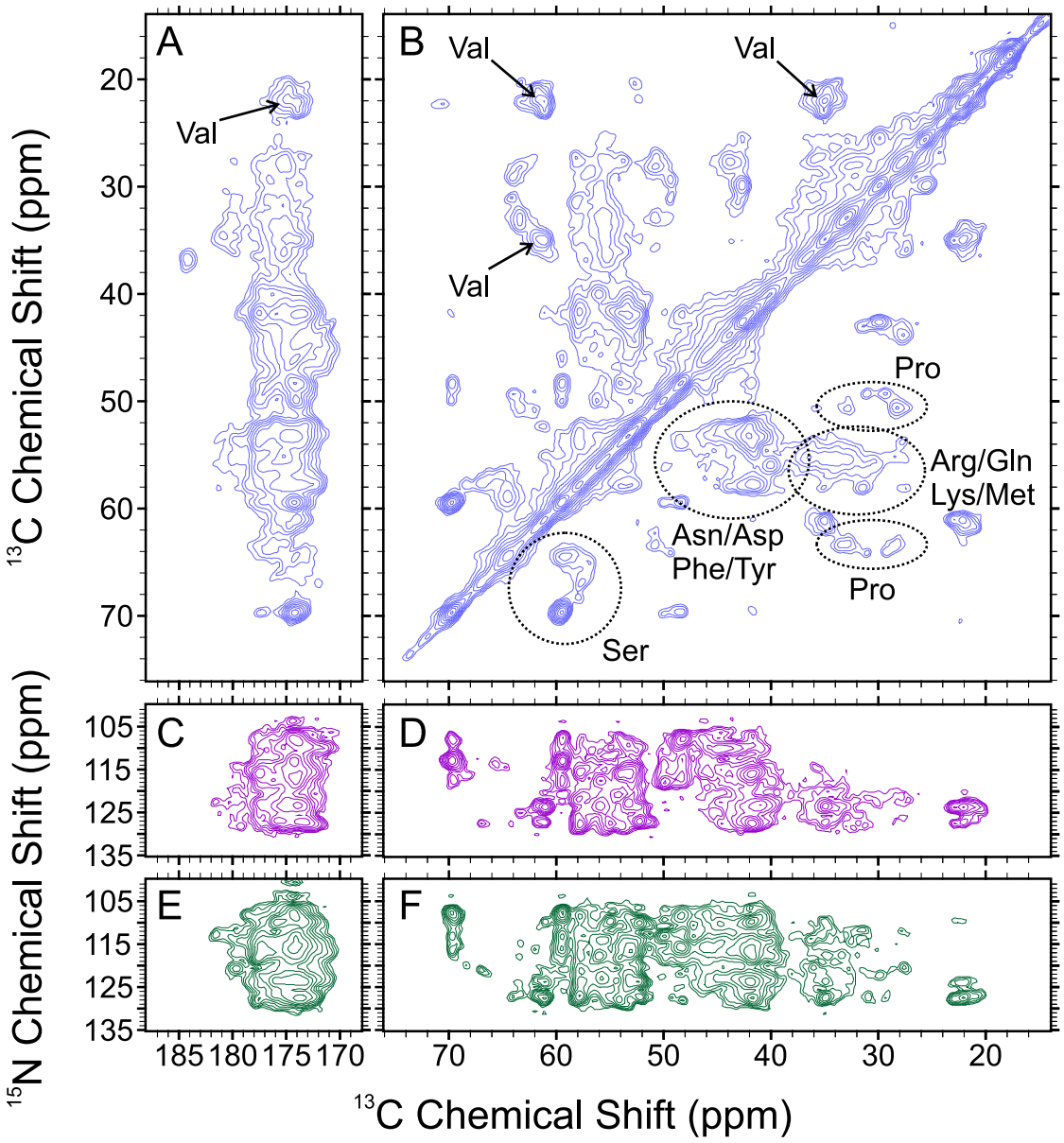
A
B
C
D
E
F
Val
Val
Val
Val
Pro
Arg/Gln
Lys/Met
Asn/Asp
Phe/Tyr
Pro
Ser
20
30
40
50
60
70
105
115
125
135
185 180 175 170
70 60 50 40 30 20
^{13}C Chemical Shift (ppm)
^{15}N Chemical Shift (ppm)
^{13}C Chemical Shift (ppm)

Figure S4

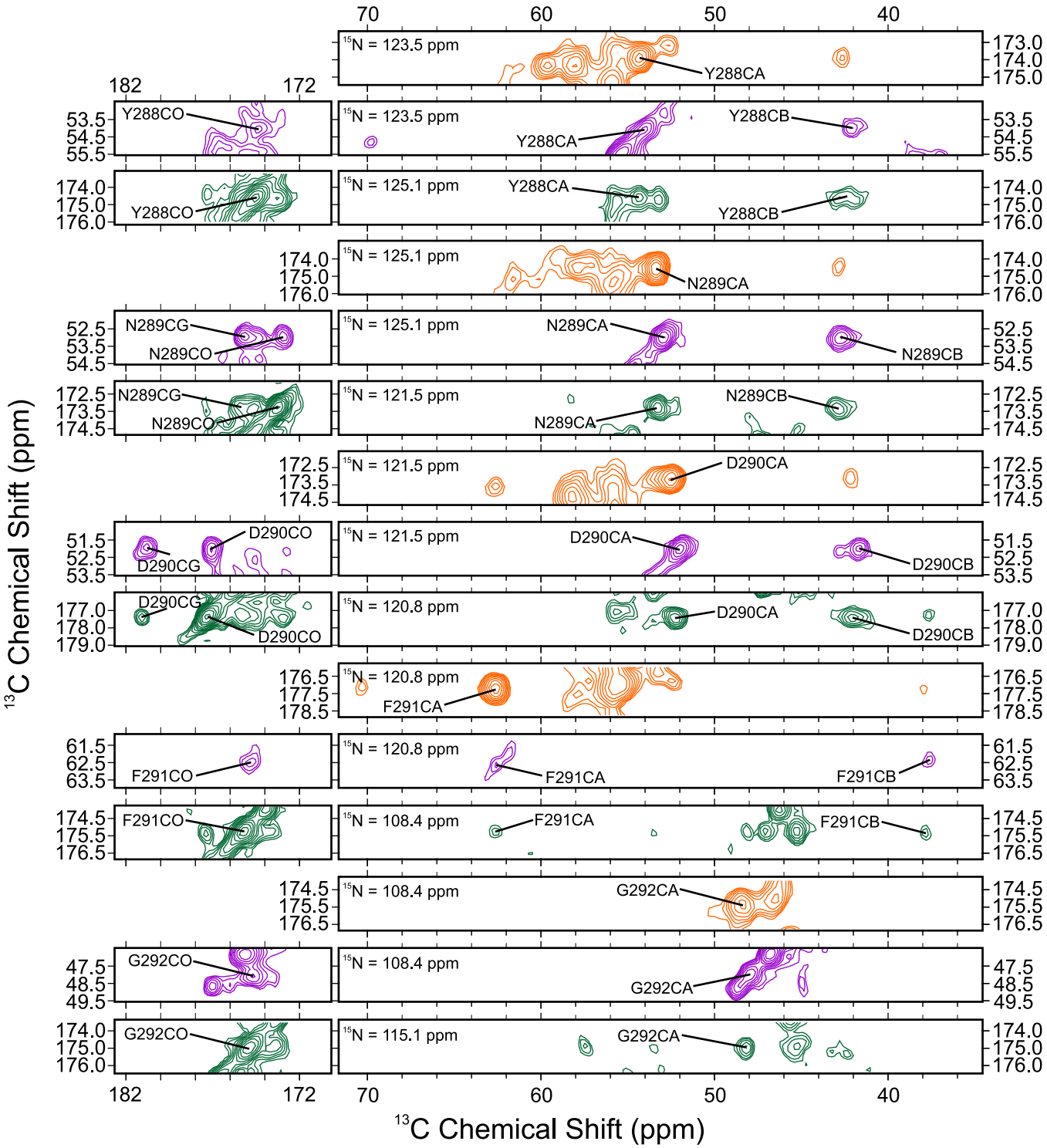
70
60
50
40
182
172
^{15}N = 123.5 ppm
Y288CA
Y288CO
Y288CB
^{15}N = 125.1 ppm
N289CA
N289CG
N289CO
N289CB
^{15}N = 121.5 ppm
D290CA
D290CG
D290CO
D290CB
^{15}N = 120.8 ppm
F291CA
F291CO
F291CB
^{15}N = 108.4 ppm
G292CA
G292CO
^{15}N = 115.1 ppm
^{13}C Chemical Shift (ppm)
^{13}C Chemical Shift (ppm)

Figure S5

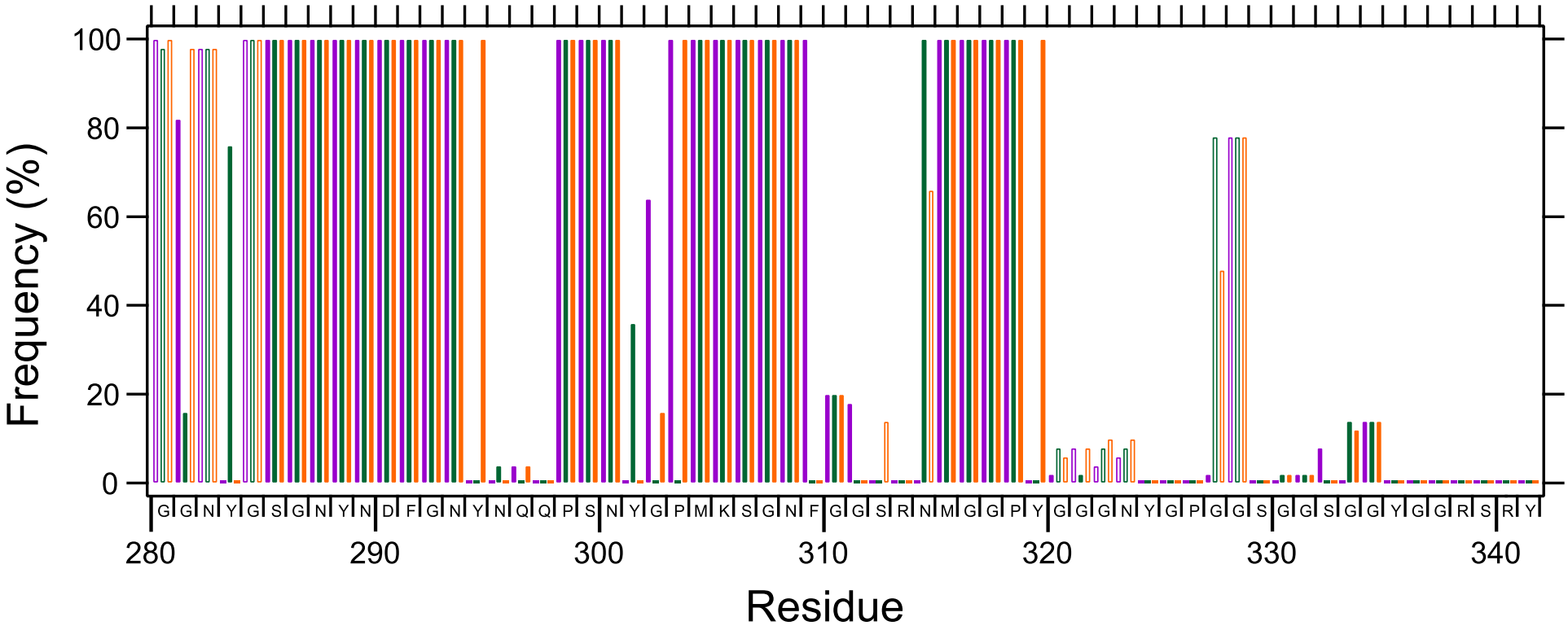
Frequency (%)
100
80
60
40
20
0
G G N Y G S G N Y N D F G N Y N Q Q P S N Y G P M K S G N F G G S R N M G G P Y G G G N Y G P G G S G G S G G Y G G R S R Y
280
290
300
310
320
330
340
Residue

Figure S6

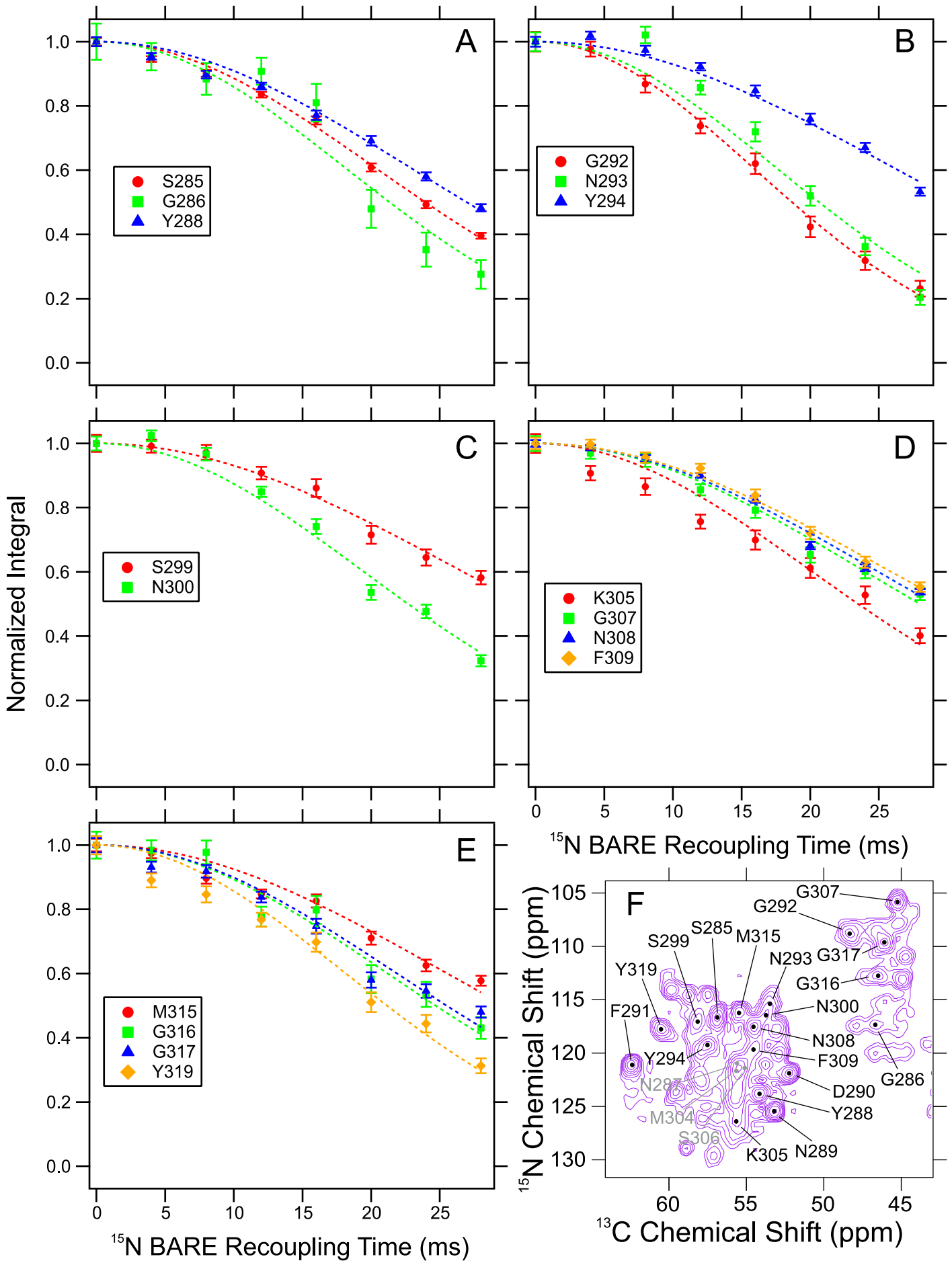
A
S285
G286
Y288
B
G292
N293
Y294
C
S299
N300
D
K305
G307
N308
F309
E
M315
G316
G317
Y319
Normalized Integral
0.0
0.2
0.4
0.6
0.8
1.0
0
5
10
15
20
25
^{15}N BARE Recoupling Time (ms)
F
G307
G292
S285
S299
M315
N293
G317
Y319
G316
F291
N300
N308
Y294
F309
G286
N287
D290
M304
Y288
S306
K305
N289
^{15}N Chemical Shift (ppm)
105
110
115
120
125
130
60
55
50
45
^{13}C Chemical Shift (ppm)

Figure S7

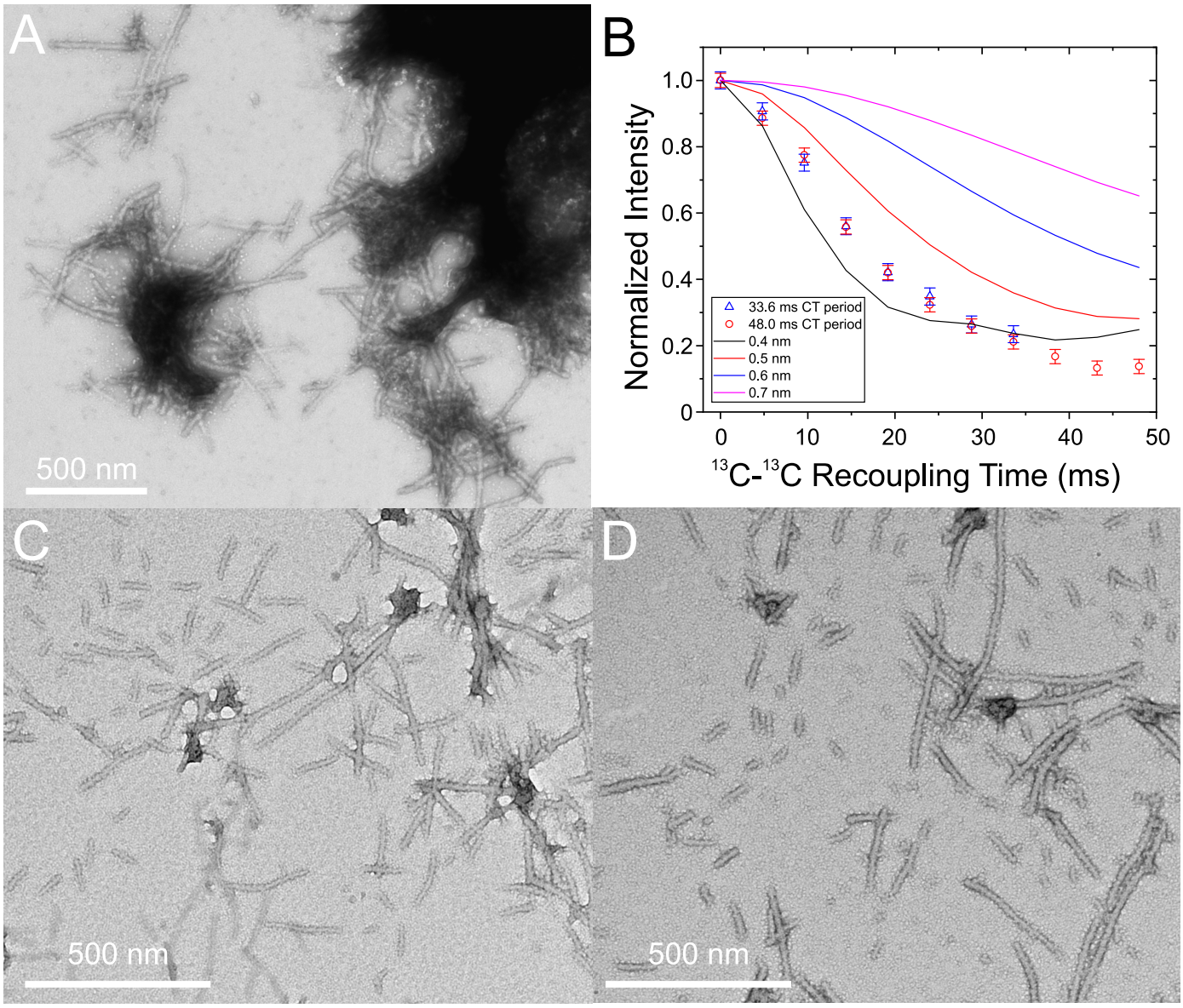
A
500 nm
B
Normalized Intensity
1.0
0.8
0.6
0.4
0.2
0
0
10
20
30
40
50
^{13}C-^{13}C Recoupling Time (ms)
33.6 ms CT period
48.0 ms CT period
0.4 nm
0.5 nm
0.6 nm
0.7 nm
C
500 nm
D
500 nm

Figure S8

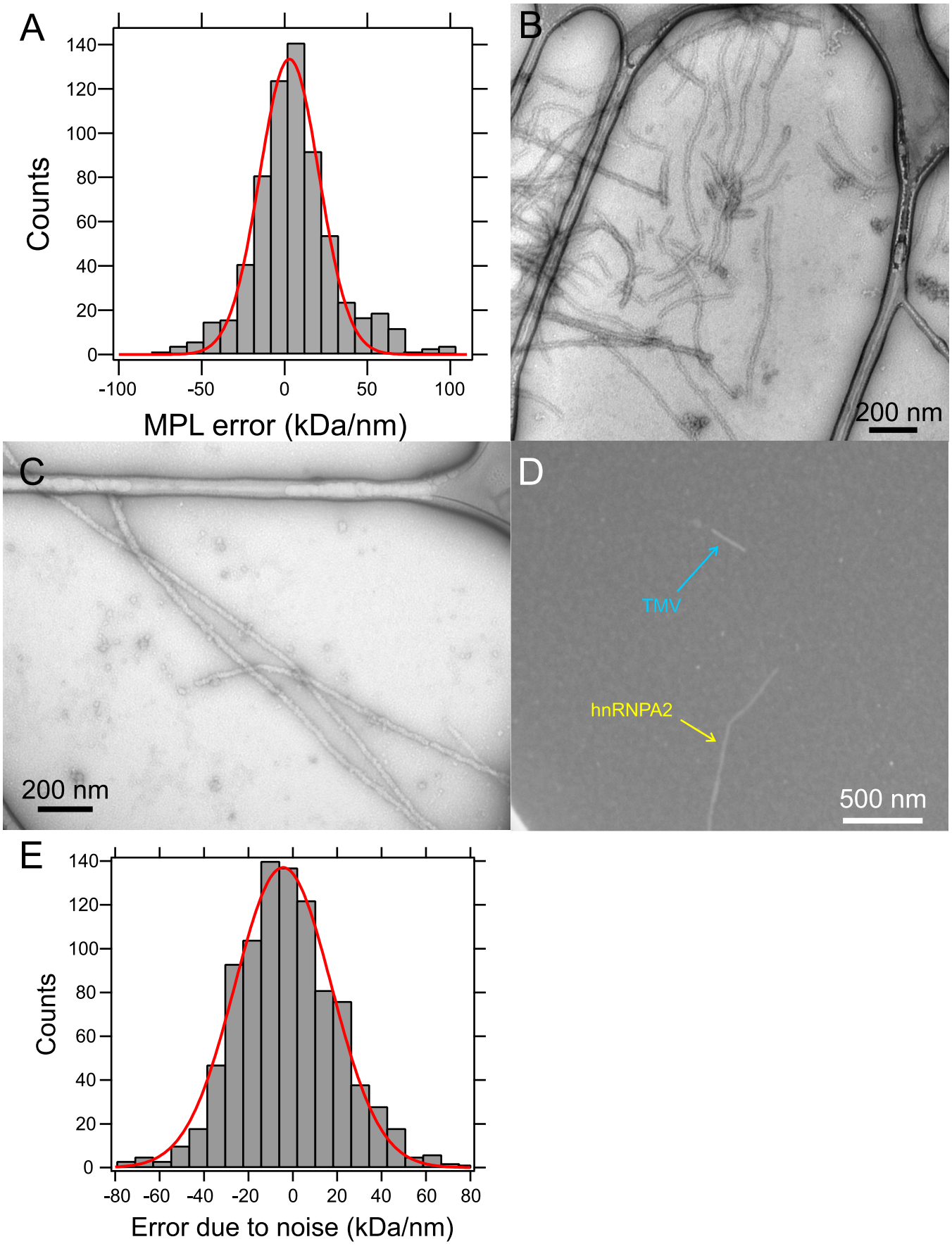
A
Counts
MPL error (kDa/nm)
B
200 nm
C
200 nm
D
TMV
hnRNPA2
500 nm
E
Counts
Error due to noise (kDa/nm)

Figure S9

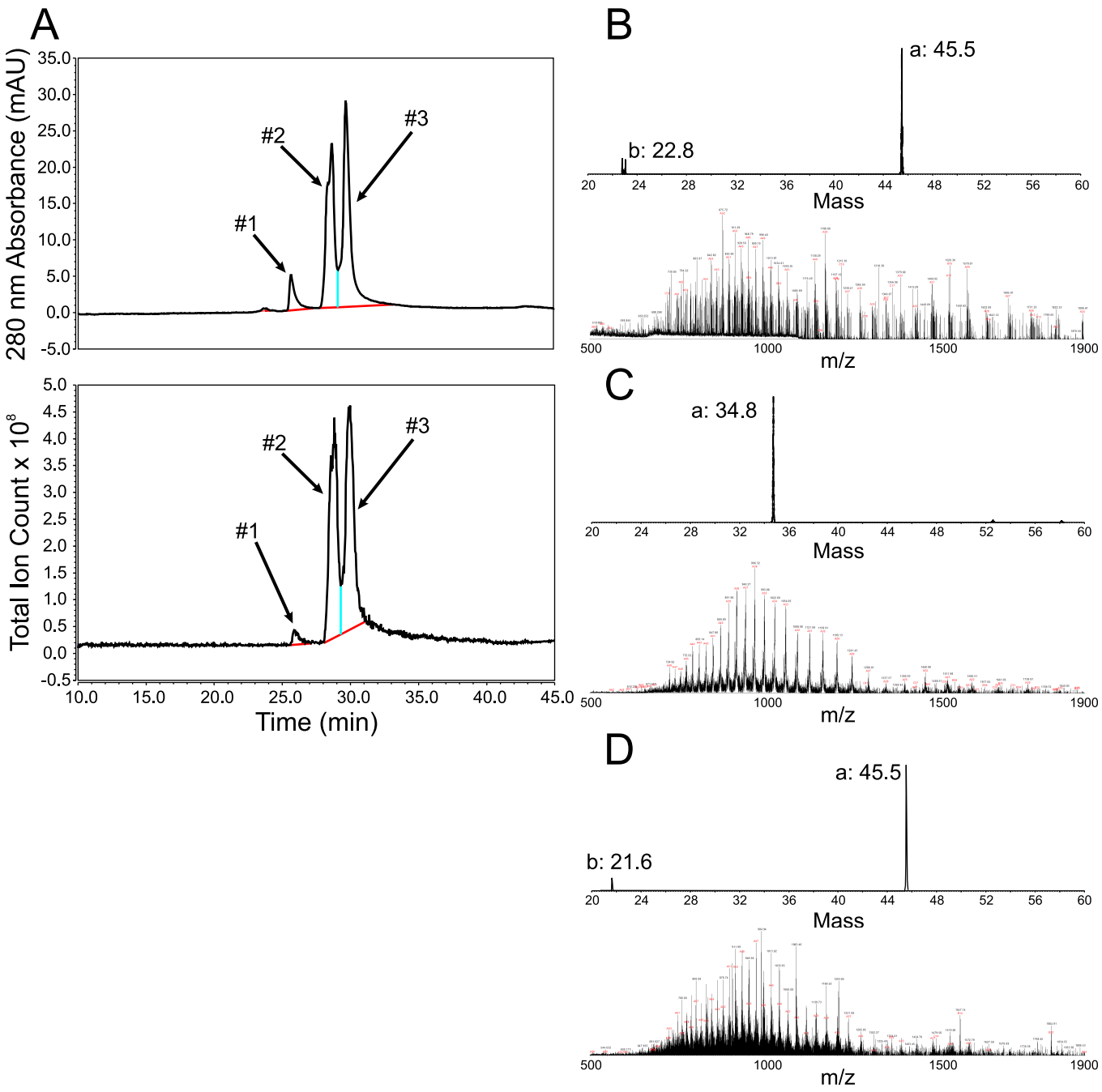
A
280 nm Absorbance (mAU)
35.0
30.0
25.0
20.0
15.0
10.0
5.0
0.0
-5.0
#1
#2
#3
Total Ion Count x 10^8
5.0
4.5
4.0
3.5
3.0
2.5
2.0
1.5
1.0
0.5
0.0
-0.5
10.0
15.0
20.0
25.0
30.0
35.0
40.0
45.0
Time (min)
B
a: 45.5
b: 22.8
20
24
28
32
36
40
44
48
52
56
60
Mass
500
1000
1500
1900
m/z
C
a: 34.8
Mass
m/z
D
a: 45.5
b: 21.6
Mass
m/z

Figure S10

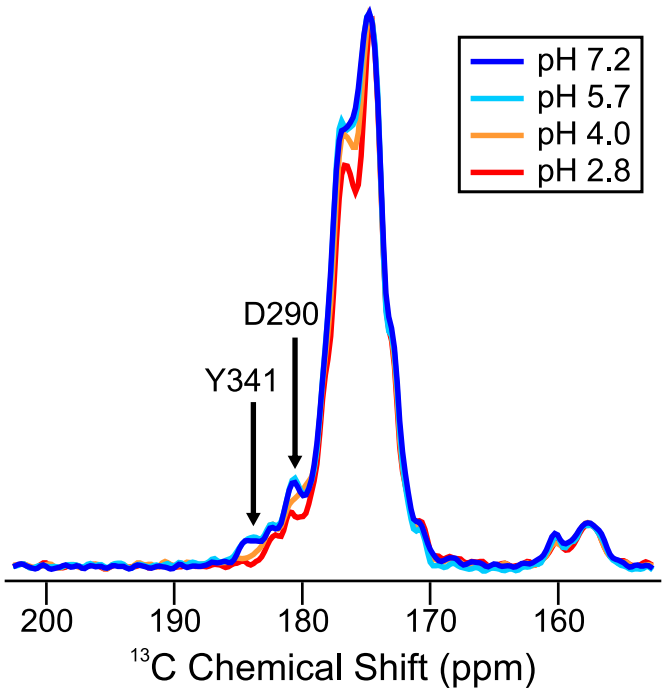
pH 7.2
pH 5.7
pH 4.0
pH 2.8
D290
Y341
200
190
180
170
160
^{13}C Chemical Shift (ppm)

Figure S11

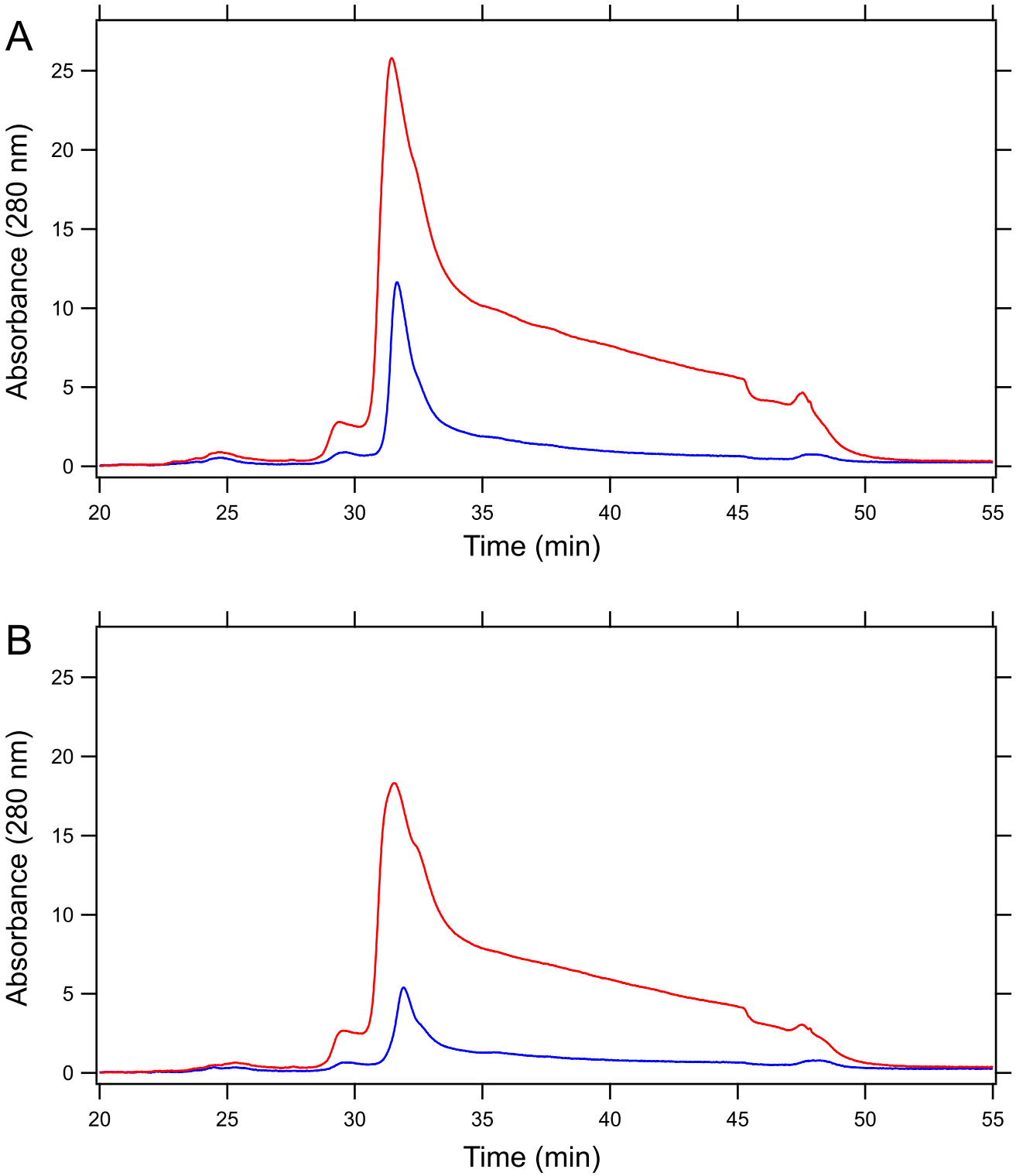
A
Absorbance (280 nm)
0
5
10
15
20
25
20
25
30
35
40
45
50
55
Time (min)
B
Absorbance (280 nm)
0
5
10
15
20
25
20
25
30
35
40
45
50
55
Time (min)

Figure S12

Supplemental Figure Captions

Figure S1: Sequence alignment of the LC domains of hnRNPs. Sequence alignments for residues 243-283 (hnRNPA1), 270-311 (hnRNPA2), and 357-398 (hnRNPDL) were performed manually. The conserved or nearly conserved residues are highlighted in bold and colored red. The aspartic acid residue mutated in multisystem proteinopathy, ALS, and limb girdle muscular dystrophy is highlighted in yellow.

Figure S2: Intein reaction scheme for the production of segmentally labeled mCherry-hnRNPA2-LC. The N-terminal portion of hnRNPA2-LC, residues 181-279, is produced with N-terminal 6x His and mCherry tags and a C-terminal Cfa intein protein linked via a cysteine residue. The Cfa intein is displaced by reaction with Mes. The C-terminal portion of hnRNPA2-LC, residues 281-341, is produced with N-terminal 6x His and mCherry tags and a caspase-3 cleavage sequence (GDEVDC). After cleavage with caspase-3 the C-terminal portion of hnRNPA2-LC has a N-terminal cysteine residue. The N-terminal and C-terminal portions of hnRNPA2-LC are mixed for the ligation reaction. The final hnRNPA2-LC product has N-terminal 6x His and mCherry tags with a cysteine substitution at residue 280. Isotopic labeling for the NMR experiments is confined to the C-terminus of hnRNPA2-LC, residues 280-341, colored red in the figure. The production of segmentally labeled D290V mutant was performed in the same method except the C-terminal labeled fragment carries the D-to-V mutation.

Figure S3: Hydrogel binding and polymer formation of the half constructs of hnRNPA2-LC and hnRNPA2-LC Thioflavin-T binding assay. (A) GFP-fused half constructs (residues 181-260 or 261-341) of hnRNPA2-LC were incubated with hydrogels of the wild type mCherry-hnRNPA2-LC (residues 181-341). Fluorescence signals of GFP-hnRNPA2-LC half constructs bound to the hydrogels were visualized by confocal microscopy. (B) TEM micrographs of GFP-fused half constructs of hnRNPA2-LC after dialysis in gelation buffer, concentration, and incubation to induce polymer formation. (C) Thioflavin-T fluorescence emission spectrum of mCherry-hnRNPA2-LC wild type polymers. (D) Thioflavin-T fluorescence emission spectrum of mCherry-hnRNPA2-LC D290V mutant polymers. In panels C and D, the solid colored, dashed colored, and gray lines represent spectra from the polymers with Thioflavin-T, polymers without Thioflavin-T, and the Thioflavin-T solution without polymers. Differences in the magnitude of the fluorescence intensities are attributable to differences in polymer concentrations and do not necessarily indicate that the wild type and D290V mutant polymers bind the Thioflavin-T dye differently. The fluorescence peak near 600 nm is a result of the overlap between Thioflavin-T emission and mCherry excitation wavelengths.

Figure S4: Solid state NMR spectra of mCherry-hnRNPA2-LC D290V mutant polymers. (A and B) 2D ^{13}C-^{13}C DARR spectrum of mCherry-hnRNPA2-LC D290V mutant polymers. Amino acid type assignments are based on the typical chemical shift ranges observed for each reside type. (C and D) 2D ^{15}N-^{13}C NCACX spectrum of mCherry-hnRNPA2-LC D290V mutant polymers. (E and F) 2D ^{15}N-^{13}C NCOCX spectrum of mCherry-hnRNPA2-LC D290V mutant polymers. For all spectra, contour levels increase by successive factors of 1.4.

Figure S5: Strip plots from 3D solid state NMR spectra of segmentally labeled mCherry-hnRNPA2-LC polymers. Portions of 2D ^{13}C-^{13}C planes from the 3D CONCA, NCACX, and

NCOCX solid state NMR spectra are shown with orange, purple, and green contours, respectively. The ^{15}N frequencies are indicated in each 2D plane. The contour levels increase by successive factors of 1.3. Assignments for residues 288-292 are shown in these strip plots.

Figure S6: MCASSIGN-based resonance assignments for segmentally labeled mCherry-hnRNPA2-LC polymers. A plot of the assignment frequencies for signals from the 3D NCACX, NCOCX, and CONCA spectra (purple, green, and orange bars, respectively) for each residue in hnRNPA2-LC, from 50 independent MCASSIGN calculations. Filled bars indicate that the same solid state NMR signals were assigned to a given residue in all calculations. Open bars indicate that different signals are assigned to a given residue in different calculations.

Figure S7: ^{15}N-BARE measurements on segmentally labeled mCherry-hnRNPA2-LC polymers. (A-E) Normalized crosspeak volumes from 2D NCA spectra as a function of the ^{15}N-BARE recoupling time. Error bars are the RMS noise in each NMR spectrum. Dashed lines are Gaussian fits to experimental data. (F) 2D NCA solid state NMR spectrum from the ^{15}N-BARE measurement with 0 ms ^{15}N recoupling time. Resolved signals are shown in black and overlapped signals are shown in gray. Contour levels increase by successive factors of 1.4.

Figure S8: Measurement of intermolecular ^{13}C-^{13}C distances in mCherry-hnRNPA2-LC polymers. (A) TEM image of segmentally ^{13}CO-Tyr-labeled mCherry-hnRNPA2-LC polymers used in the ^{13}C PITHIRDS-CT measurement shown in Fig. 4D, negatively stained with uranyl acetate. (B) ^{13}C-^{13}C PITHIRDS-CT curves for segmentally ^{13}CO-Tyr labeled mCherry-hnRNPA2-LC D290V polymers. The curves are simulated data for linear chains of ^{13}C-labeled atoms with the interatomic distances indicated in the figure. (C) TEM image of segmentally ^{13}CO-Tyr-labeled mCherry-hnRNPA2-LC D290V polymers. (D) TEM image of segmentally ^{15}N,^{13}C-labeled mCherry-hnRNPA2-LC D290V polymers.

Figure S9: Mass-per-length measurements on mCherry-hnRNPA2-LC wild type and D290V mutant polymers. (A) Histogram of variations in integrated background intensities in the dark-field images used for mass-per-length measurements in Fig. 5. The red line is a Gaussian fit to the data centered, at 2.9 ± 0.9 kDa/nm with a width of 25.4 ± 1.2 kDa/nm. (B) TEM image of negatively stained mCherry-hnRNPA2-LC polymers used in the MPL measurements shown in Fig. 5. (C) TEM micrograph of negatively stained mCherry-hnRNPA2-LC D290V polymers (D) Dark-field TEM image of unstained mCherry-hnRNPA2-LC D290V polymers. mCherry-hnRNPA2-LC-D290V polymers are indicated with yellow arrows and TMV particles are indicated with cyan arrows. (E) Histogram of variations in the integrated background intensities in dark-field images of the mCherry-hnRNPA2-LC-D290V polymers. The red line is a Gaussian fit to the data, centered at -4.4 ± 0.8 kDa/nm with a width of 30.8 ± 1.1 kDa/nm.

Figure S10: Mass measurement on monomers in the mCherry-hnRNPA2-LC polymers. (A) Chromatographic traces of the eluate from a C4 column of the mCherry-hnRNPA2-LC polymers resuspended in chemical denaturant. The top panel is the absorbance at 280 nm and the bottom panel is the total ion count measured by the mass detector. Two major and one minor peak are detected in both traces. (B-D) The top panels are the deconvolved mass spectra and the bottom

panels are the raw m/z spectra. (B) is peak #1, (C) is peak #2, and (D) is peak #3, as indicated in panel (A).

Figure S11: Charge state of D290 in mCherry-hnRNPA2-LC polymers.
Carbonyl/carboxylate regions of 1D solid state NMR spectra of mCherry-hnRNPA2-LC polymers at pH 2.8, 4.0, 5.7, and 7.2. The carboxylate signals for the D290 sidechain C_γ and the Y341 backbone CO sites are indicated in the figure.

Figure S12: HPLC chromatograms of soluble GFP-hnRNPA2-LC after polymers were exposed to urea. Red curves are soluble GFP-hnRNPA2-LC at 4.5 M urea and blue curves are soluble GFP-hnRNPA2-LC at 2.5 M urea. (A) is the wild-type protein and (B) is the D290V mutant protein.

Table S1. Amino acid compositions of full-length hnRNPA2-LC and the segmentally labeled segment.

	Residues 181-341		**Residues 280-341**	
Amino Acid	**Number**	**Percent**	**Number**	**Percent**
Ala	0	0	0	0
Arg	9	5.6	3	4.8
Asn	16	9.9	9	14.5
Asp	5	3.1	1	1.6
Cys	0	0	0	0
Gln	5	3.1	2	3.2
Glu	1	0.6	0	0
Gly	71	44.1	23	37.1
His	0	0	0	0
Ile	0	0	0	0
Leu	0	0	0	0
Lys	1	0.6	1	1.6
Met	3	1.9	2	3.2
Phe	8	5.0	2	3.2
Pro	9	5.6	4	6.5
Ser	15	9.3	7	11.3
Thr	0	0	0	0
Trp	0	0	0	0
Tyr	17	10.6	8	12.9
Val	1	0.6	0	0
Total	**161**		**62**	

Table S2. Chemical shift assignments for signals observed in the 3D solid state NMR spectra of segmentally labeled mCherry-hnRNPA2-LC polymers. ^{15}N chemical shifts are in ppm relative to liquid ammonia. ^{13}C chemical shifts are in ppm relative to DSS.

Residue	^{15}N	$^{13}C_{\alpha}$	^{13}CO	$^{13}C_{\beta}$	$^{13}C_{\gamma}$	$^{13}C_{\delta}$
S285	116.2	56.8	176.3	66.3		
G286	117.0	47.0	175.4			
N287	120.7	55.6	173.9	41.6	177.2	
Y288	123.5	54.2	174.5	42.4		
N289	125.2	53.2	173.1	42.7	175.2	
D290	121.5	52.2	177.2	41.8	180.9	
F291	120.8	62.6	175.2	37.7		
G292	108.2	48.2	175.0			
N293	115.1	53.6	178.5	42.6		
Y294	118.6	57.6				
P298	133.3	63.0	176.9	32.4	28.8	49.2
S299	116.4	58.3	176.5	69.2		
N300	116.7	53.5	172.6	41.1		
P303	134.7	63.3	176.8	32.3	28.9	49.4
M304	121.1	55.6	175.1	34.0	30.0	
K305	126.1	55.7	176.4	36.3		
S306	121.1	55.0	176.9	70.3		
G307	105.1	45.4	176.2			
N308	117.3	54.5	174.8	39.1	176.8	
F309	118.9	54.2	174.0	41.7		
N314		52.9	178.4	40.4		
M315	115.7	55.4	178.1	38.5	33.2	
G316	112.3	46.4	173.8			
G317	109.3	46.0	170.7			
P318	137.7	63.8	178.5	32.0	29.6	51.134
Y319	117.3	60.6				

Table S3. Chemical shift values for unassigned signals observed in the 3D NCACX, NCOCX, and CONCA solid state NMR spectra of segmentally labeled mCherry-hnRNPA2-LC polymers. ^{15}N chemical shifts are in ppm relative to liquid ammonia. ^{13}C chemical shifts are in ppm relative to DSS.

NCACX					
Residue Type	**^{15}N**	**$^{13}C_\alpha$**	**^{13}CO**	**$^{13}C_\beta$**	**$^{13}C_\gamma$**
G	107.4	44.8	171.3		
G	107.9	48.7	177.0		
G	108.0	46.8	175.1		
G	110.5	44.8	174.2		
G	112.8	44.9	174.7		
S	114.1	57.3	173.5	67.6	
S	114.3	58.5	172.9	67.6	
G	115.1	45.3	173.0		
G	117.2	47.4	174.0		
N	117.5	52.6	173.9	40.1	178.2
N	119.5	52.7	174.6	44.3	177.5
G	119.5	46.1	173.9		
S	123.4	54.8	176.5	69.7	
Q	123.9	55.5	175.0	31.5	38.0
NCOCX					
Residue Type	**^{15}N**	**$^{13}C_\alpha$**	**^{13}CO**	**$^{13}C_\beta$**	**$^{13}C_\gamma$**
G	108.1	47.0	175.3		
G	108.5	45.2	175.2		
NYF	110.5	52.8	174.3	40.5	
NYF	111.8	53.2	175.5	43.0	
G	112.7	48.9	177.4		
NYF	113.7	52.9	174.9		
G	116.1	45.5	173.2		
G	116.5	45.0	174.7		
NYF	116.9	54.4	177.5	41.7	
G	117.2	47.2	176.4		
NYF	118.0	55.6	177.7	41.7	
NYF	120.0	53.5	176.0	45.3	
G	120.5	47.1	175.5		
NYFMKRS	121.3	55.4	174.8		
NYFMKRS	124.3	55.7	175.6		
CONCA					
Residue Type	**^{15}N**	**$^{13}C_\alpha$**	**^{13}CO**	**$^{13}C_\beta$**	**$^{13}C_\gamma$**
G	107.0	45.3	177.4		
G	108.2	46.6	175.1		
G	108.0	48.7	175.9		
G	110.2	44.8	174.5		
G	112.5	45.1	177.8		
S	113.9	57.6	176.4		
S	114.0	58.8	177.1		

G	115.1	46.1	174.8		
S	116.1	57.0	172.9		
S	116.3	57.1	174.5		
N	116.9	54.8	172.9		
G	117.0	47.9	176.4		
NYF	117.3	53.2	176.4		
NYF	119.0	54.6	173.5		
N	119.5	53.0	175.6		
G	119.7	46.3	177.1		
KM	120.9	55.7	175.5		
NYFMKRSQ	121.9	58.1	174.3		
Q	123.5	55.8	175.5		

Table S4. Parameters for the acquisition and processing of the NMR spectra.

Experiment	Parameters	Processing
Sample: Uniform-[^{13}C,^{15}N] mCherry-hnRNPA2-LC polymers		
1D *fs*-REDOR	B_0 = 14.1 T; na = 768; ν_{MAS} = 12 kHz; $\nu_{H\pi/2}$ = 58 kHz; ν_{HCP} = 63 kHz; ν_{CCP} = 50 kHz; ν_{HDEC} = 84 kHz; ν_{Cgauss} = 5 kHz; ν_{NRFDR} = 50 kHz; τ_{HC} = 1.5 ms; τ_{acq} = 7.7 ms; τ_{dwell} = 15 µs; τ_{REDOR} = 1.33 ms; τ_{pd} = 2 s;	t_1: GB = 125 Hz
2D CC DARR	B_0 = 14.1 T; na = 192; ν_{MAS} = 12 kHz; $\nu_{H\pi/2}$ = 58 kHz; ν_{HCP} = 63 kHz; ν_{CCP} = 50 kHz; ν_{HDEC} = 84 kHz; ν_{DARR} = 12 kHz; $\nu_{C\pi/2}$ = 50 kHz; τ_{HC} = 1.5 ms; τ_{DARR} = 50 ms; τ_{dwell} = 15 µs; τ_{acq} = 7.7 ms; t_{1max} = 5.8 ms; t_{1inc} = 24 µs; τ_{pd} = 2 s;	t_2: GB = 100 Hz t_1: GB = 100 Hz
2D NCACX	B_0 = 14.1 T; na = 640; ν_{MAS} = 12 kHz; $\nu_{H\pi/2}$ = 58 kHz; ν_{HCP1} = 57 kHz; ν_{NCP1} = 47 kHz; ν_{NCP2} = 4 kHz; ν_{CCP2} = 16 kHz; ν_{HDEC} = 84 kHz; ν_{DARR} = 12 kHz; $\nu_{C\pi/2}$ = 50 kHz; τ_{HC} = 1.5 ms; τ_{NC} = 4 ms; τ_{DARR} = 50 ms; τ_{dwell} = 15 µs; τ_{acq} = 7.7 ms; t_{1max} = 4.6 ms; t_{1inc} = 84 µs; τ_{pd} = 2 s;	t_2: none t_1: LP = 44 points
2D NCOCX	B_0 = 14.1 T; na = 640; ν_{MAS} = 12 kHz; $\nu_{H\pi/2}$ = 58 kHz; ν_{HCP1} = 57 kHz; ν_{NCP1} = 47 kHz; ν_{NCP2} = 27 kHz; ν_{CCP2} = 39 kHz; ν_{HDEC} = 84 kHz; ν_{DARR} = 12 kHz; $\nu_{C\pi/2}$ = 50 kHz; τ_{HC} = 1.5 ms; τ_{NC} = 4 ms; τ_{DARR} = 50 ms; τ_{dwell} = 15 µs; τ_{acq} = 7.7 ms; t_{1max} = 4.6 ms; t_{1inc} = 84 µs; τ_{pd} = 2 s;	t_2: none t_1: LP = 44 points
3D NCACX	B_0 = 14.1 T; na = 48; ν_{MAS} = 12 kHz; $\nu_{H\pi/2}$ = 58 kHz; ν_{HCP1} = 57 kHz; ν_{NCP1} = 47 kHz; ν_{NCP2} = 15 kHz; ν_{CCP2} = 27 kHz; ν_{HDEC} = 84 kHz; ν_{DARR} = 12 kHz; $\nu_{C\pi/2}$ = 50 kHz; τ_{HC} = 1.5 ms; τ_{NC} = 4 ms; τ_{DARR} = 50 ms; τ_{dwell} = 15 µs; τ_{acq} = 7.7 ms; t_{1max} = 8.0 ms; t_{1inc} = 150.8 µs; t_{2max} = 6.0 ms; t_{2inc} = 104.4 µs; τ_{pd} = 1.3 s;	t_3: GB = 50 Hz t_2: GB = 50 Hz t_1: GB = 30 Hz
3D NCOCX	B_0 = 14.1 T; na = 240; ν_{MAS} = 12 kHz; $\nu_{H\pi/2}$ = 58 kHz; ν_{HCP1} = 57 kHz; ν_{NCP1} = 47 kHz; ν_{NCP2} = 4 kHz; ν_{CCP2} = 16 kHz; ν_{HDEC} = 84 kHz; ν_{DARR} = 12 kHz; $\nu_{C\pi/2}$ = 50 kHz; τ_{HC} = 1.5 ms; τ_{NC} = 4 ms; τ_{DARR} = 50 ms; τ_{dwell} = 15 µs; τ_{acq} = 7.7 ms; t_{1max} = 8.0 ms; t_{1inc} = 150.8 µs; t_{2max} = 6.0 ms; t_{2inc} = 150.8 µs; τ_{pd} = 1.3 s;	t_3: GB = 50 Hz t_2: GB = 50 Hz t_1: GB = 30 Hz
3D CONCA	B_0 = 17.5 T; na = 96; ν_{MAS} = 12 kHz; $\nu_{H\pi/2}$ = 63 kHz; ν_{HCP1} = 62 kHz; ν_{CCP1} = 74 kHz; ν_{NCP2} = 17 kHz; ν_{CCP2} = 29 kHz; ν_{NCP3} = 17 kHz; ν_{CCP3} = 29 kHz; ν_{HDEC} = 85 kHz; τ_{HC} = 1.5 ms; τ_{NC} = 4 ms; τ_{dwell} = 15 µs; τ_{acq} = 7.7 ms; t_{1max} = 3.4 ms; t_{1inc} = 176.4 µs; t_{2max} = 5.3 ms; t_{2inc} = 100.8 µs; τ_{pd} = 1.3 s;	t_3: GB = 100 Hz t_2: GB = 20 Hz t_1: GB = 10 Hz
2D BARE	B_0 = 17.5 T; na = 128; ν_{MAS} = 12 kHz; $\nu_{H\pi/2}$ = 63 kHz; ν_{HCP1} = 57 kHz; ν_{NCP1} = 35 kHz; ν_{NCP2} = 17 kHz; ν_{CCP2} = 29 kHz; ν_{HDEC} = 85 kHz; ν_{NBARE} = 18 kHz; τ_{HC} = 1.5 ms; τ_{NC} = 4 ms; $\tau_{BAREinc}$ = 4 ms; $\tau_{BAREtotal}$ = 28 ms; τ_{dwell} = 15 µs; τ_{acq} = 5.5 ms; t_{1max} = 8.4 ms; t_{1inc} = 100.8 µs; τ_{pd} = 2.3 s;	t_2: GB = 20 Hz t_1: GB = 10 Hz
Sample: Uniform-[^{13}C,^{15}N] mCherry-hnRNPA2-LC D290V polymers		
2D CC DARR	B_0 = 17.5 T; na = 192; ν_{MAS} = 12 kHz; $\nu_{H\pi/2}$ = 62.5 kHz; ν_{HCP} = 58 kHz; ν_{CCP} = 43 kHz; ν_{HDEC} = 85 kHz; ν_{DARR} = 12 kHz; $\nu_{C\pi/2}$ = 50 kHz; τ_{HC} = 1.5 ms; τ_{DARR} = 50 ms; τ_{dwell} = 15 µs; τ_{acq} = 7.7 ms; t_{1max} = 5.8 ms; t_{1inc} = 22.4 µs; τ_{pd} = 1.5 s;	t_2: GB = 100 Hz t_1: GB = 100 Hz
2D NCACX	B_0 = 17.5 T; na = 1664; ν_{MAS} = 12 kHz; $\nu_{H\pi/2}$ = 62.5 kHz; ν_{HCP1} = 62 kHz; ν_{NCP1} = 36 kHz; ν_{NCP2} = 19.2 kHz; ν_{CCP2} = 31.2 kHz; ν_{HDEC} = 85 kHz; ν_{DARR} = 12 kHz; $\nu_{C\pi/2}$ = 50 kHz; τ_{HC} = 1.5 ms; τ_{NC} = 4 ms; τ_{DARR} = 50 ms; τ_{dwell} = 15 µs; τ_{acq} = 7.7 ms; t_{1max} = 4.6 ms; t_{1inc} = 82.6 µs; τ_{pd} = 1.5 s;	t_2: GB = 90 Hz t_1: none
2D NCOCX	B_0 = 17.5 T; na = 1664; ν_{MAS} = 12 kHz; $\nu_{H\pi/2}$ = 62.5 kHz; ν_{HCP1} = 62 kHz; ν_{NCP1} = 36 kHz; ν_{NCP2} = 28.8 kHz; ν_{CCP2} = 40.8 kHz; ν_{HDEC} = 84 kHz; ν_{DARR} = 12 kHz; $\nu_{C\pi/2}$ = 50 kHz; τ_{HC} = 1.5 ms; τ_{NC} = 4 ms; τ_{DARR} = 50 ms; τ_{dwell} = 15 µs; τ_{acq} = 7.7 ms; t_{1max} = 4.6 ms; t_{1inc} = 82.6 µs; τ_{pd} = 1.5 s;	t_2: GB = 90 Hz t_1: none
Samples: ^{13}CO-Tyr mCherry-hnRNPA2-LC polymers		
1D CC PITHIRDS-CT	B_0 = 9.4 T; na = 2048; ν_{MAS} = 18 kHz; $\nu_{H\pi/2}$ = 63 kHz; ν_{HCP1} = 75 kHz; ν_{CCP1} = 56 kHz; ν_{HDEC} = 100 kHz; $\nu_{CPITHIRDS}$ = 27 kHz; $\nu_{CSPINLOCK}$ = 42	t_1: LB = 10 Hz

	kHz; τ_{HC} = 1.5 ms; $\tau_{PITHIRDSinc}$ = 5.3 ms; $\tau_{PITHIRDStotal}$ = 42.4 ms; τ_{dwell} = 20 µs; τ_{acq} = 20.5 ms; τ_{pd} = 4.0 s;	
Sample: ^{13}CO-Tyr mCherry-hnRNPA2-LC D290V polymers		
1D CC PITHIRDS-CT	B_0 = 9.4 T; na = 2048; ν_{MAS} = 20 kHz; $\nu_{H\pi/2}$ = 63 kHz; ν_{HCP1} = 70 kHz; ν_{CCP1} = 50 kHz; ν_{HDEC} = 102 kHz; $\nu_{CPITHIRDS}$ = 30 kHz; $\nu_{CSPINLOCK}$ = 40 kHz; τ_{HC} = 1.5 ms; $\tau_{PITHIRDSinc}$ = 4.8 ms; $\tau_{PITHIRDStotal}$ = 33.6 or 48.0 ms; τ_{dwell} = 5 µs; τ_{acq} = 25.6 ms; τ_{pd} = 4.0 s;	t_1: LB = 20 Hz
Samples: Uniform-[^{13}C,^{15}N] mCherry-hnRNPA2 polymers (pH 2.8, 4.0, 5.7, 7.2)		
1D CPMAS	B_0 = 14.1 T; na = 12288; ν_{MAS} = 13.6 kHz; $\nu_{H\pi/2}$ = 50 kHz; ν_{HCP} = 50 kHz; ν_{CCP} = 36 kHz; ν_{HDEC} = 80 kHz; τ_{HC} = 1.5 ms; τ_{acq} = 7.7 ms; τ_{dwell} = 15 µs; τ_{pd} = 2 s;	t_1: none
2D CC DARR	B_0 = 14.1 T; na = 1152 (2304*); ν_{MAS} = 13.6 kHz; $\nu_{H\pi/2}$ = 50 kHz; ν_{HCP} = 50 kHz; ν_{CCP} = 36 kHz; ν_{HDEC} = 80 kHz; ν_{DARR} = 14 kHz; $\nu_{C\pi/2}$ = 50 kHz; τ_{HC} = 1.5 ms; τ_{DARR} = 50 ms; τ_{dwell} = 15 µs; τ_{acq} = 7.7 ms; t_{1max} = 2.6 ms; t_{1inc} = 23.2 µs; τ_{pd} = 1 s;	t_2: GB = 100 Hz t_1: GB = 100 Hz

*The CC DARR spectrum of the pH 2.9 and pH 7.3 samples averaged 1152 and 2304 acquisitions, respectively.

Abbreviations: B_0 = NMR magnetic field; na = number of acquisitions averaged; ν_{MAS} = sample spinning frequency; $\nu_{H\pi/2}$ = ^{1}H π/2 pulse strength; $\nu_{C\pi/2}$ = ^{13}C π/2 pulse strength; ν_{XCP} = cross polarization strength on nucleus 'X' (X = ^{1}H, ^{13}C, or ^{15}N). Numbered subscripts refer to the ordering of multiple cross polarization transfers in the NMR experiment; ν_{HDEC} = ^{1}H decoupling strength; ν_{Cgauss} = ^{13}C gaussian pulse strength; ν_{NRFDR} = ^{15}N π pulse strength during RFDR mixing; ν_{DARR} = DARR ^{1}H pulse strength; ν_{NBARE} = ^{15}N π pulse during the ^{15}N-BARE mixing period; $\nu_{CPITHIRDS}$ = ^{13}C π pulse during ^{13}C-^{13}C PITHIRDS-CT mixing period; $\nu_{CSPINLOCK}$ = spin lock ^{13}C π pulse for the ^{13}C-^{13}C PITHIRDS-CT experiment; τ_{HC} = ^{1}H-^{13}C cross polarization mixing time; τ_{HN} = ^{1}H-^{15}N cross polarization mixing time; τ_{NC} = ^{15}N-^{13}C cross polarization mixing time; τ_{acq} = acquisition time; τ_{dwell} = dwell time; τ_{REDOR} = increment for the *fs*-REDOR mixing period; $\tau_{BAREinc}$ = recoupling increment for ^{15}N-BARE mixing; $\tau_{BAREtotal}$ = constant time block length for the ^{15}N-BARE experiment; $\tau_{PITHIRDSinc}$ = recoupling increment for the ^{13}C-^{13}C PITHIRDS-CT mixing period; $\tau_{PITHIRDStotal}$ = constant time block length for the ^{13}C-^{13}C PITHIRDS-CT experiment; t_{1max} = maximum acquisition time in the first indirect dimension; t_{1inc} = increment for the first indirect dimension; t_{2max} = maximum acquisition time in the second indirect dimension; t_{2inc} = increment for the second indirect dimension; τ_{pd} = pulse delay; LP = linear prediction; GB = gaussian line broadening; LB = lorentizan line broadening;